Renewable Energy, Environment, and Power Quality Journal (REE&PQJ)
ISSN:3020-531X
Volume No.2, July 2024

Optimal Lithium-Ion Ageing Mechanisms Configuration for Physics-Based Modelling Software

S. Obrador[1,2], L. Canals[2] and L. Trilla[1]

[1] Power Systems, Catalonia Institute for Energy Research (IREC), Jardins de les Dones de Negre 1, 2ª pl. 08930 Sant Adrià del Besòs, Barcelona, Spain
[2] Project and Construction Engineering Department, Universitat Politècnica de Catalunya (UPC), Campus Diagonal Sud, ETSEIB Building H, Av. Diagonal, 647, 08024 Barcelona

Abstract. Reduced-order physics-based models hold the potential for enhancing the performance and extending the lifespan of lithium-ion batteries in practical battery management system applications. However, there is an urgent need to establish a correlation framework between these models and the integration of robust adaptative aging mechanisms that represent the electrochemical domain. This article uses SPM parameters and real experimental data to emulate different adaptive block configurations. Aiming to define their requirements and optimal applicability. Results show that electrode diffusivity, particle radius, and the proper identification of its boundaries, are the keys to obtaining physically meaningful results with adaptative ageing mechanisms.

Key words. Lithium-Ion, Ageing Mechanisms, Physics-Based Models, Battery Management Systems.

1. Introduction

The integration of Lithium-Ion Batteries (LIB), alongside renewable energy resources, presents a compelling strategy to enhance power grid quality applications [1]. However, sustainability poses a significant challenge for LIB. A crucial aspect in addressing this issue is the improvement of Battery Management Systems (BMS) modelling software technology [2]. These advancements aim to provide more accurate State-of-X (SoX) estimations to extend the usage and lifespan of LIB [2].

Nowadays, Equivalent Circuit Models (ECM) stand as the predominant approach for estimating principal SoX parameters: State-of-Charge (SoC) [3], and State-of-Health (SoH) [4] as the main outputs. ECM's popularity arises from their simplicity and low computational requirements [4]. Nevertheless, the lack of physical insight hinders their ability to capture the intricate transport dynamics and degradation mechanisms governing lithium-ions within cells [3].

By using the Pseudo-two-dimensional (P2D) approach, Physics-based models have the potential to compete with advanced ECM, simulating accurately the lithium-ion exchange in phases depending on the cell's macroscopic structure [5]. The most renowned among P2D models is the Doyle-Fuller-Newman (DFN) model, which provides valuable physical insights through its implementation. However, its demanding computational requirements make it impractical for control-oriented applications [6]. Consequently, it becomes necessary to explore Reduced Order Model (ROM) approaches to unlock the potential of physics-based models to run in BMS [7], [8].

Research in P2D ROM has mainly focused on refining the non-linearities of DFN's simplest derivation, the Single Particle Model (SPM), to keep P2D physical insight and low computational requirements [9]. The goal has been to closely align these non-linearities with the continuum framework characterising the partial differential equations governing LIB [7]. Additionally, SPM advancements have been complemented with the integration of filter-based methods to enhance the accuracy of SoX estimation [10].

However, due to filter parameter adjustability limitations, it is necessary to develop complementary adaptive techniques for BMS [3], [4]. These techniques, rooted in Machine Learning (ML) optimization approaches [11] such as Least Squares (LS), Gradient-Descent (GD), and Bayesian methods [11], can identify the changes of P2D ROM parameters throughout different stages of LIB degradation [12].

Proper filter-based state estimation and complementary adaptative techniques have the potential to enable the integration of robust and reliable ageing mechanisms for P2D LIB models [7], [8], by enhancing the accuracy of SoX predictions in real-time. However, the investigation into adaptive mechanisms for P2D ROM is still in its early stages [12].

Up to date, the few approaches to reduce the model used a physics-based Equivalent Hydraulic Model (EHM) derived from SPM, and an Extended Kalman Filter (EKF) as negative electrode system observers, combined with an adaptive parameter estimation block [12], [13]. Based on LS optimization method the adaptative block estimates EHM particle radius and solid diffusivity, leaving the rest untouched [12], [13]. This approach, although relatively effective in terms of adjusting model outputs, lacks physical sense, as diffusivity results from the estimation increase, instead of following the expected decreasing trend throughout degradation [14], which is confusing considering that they use physic-based models to be more realistic. Hence, it is needed to adapt the parameters within coherent values.

Therefore, there is a gap between SPM's parameter adaptive mechanisms and the electrochemical domain represented by P2D models. The present study aims to bridge this existing gap. To do so, the evolution SPM parameter is assessed over degradation. LGM50-T cell is used as a reference, fitting its SPM model [15] with degradation experimental data [16] in different parameter identification scenarios.

By emulating an adaptative block, the results from these scenarios define the requirements and the optimal configuration for the implementation of ageing mechanisms in the P2D ROM context. These insights prove essential for advancing the development of the next generation of BMS models.

2. Materials and Methods

The procedure outlined in this article involves two key aspects. First, the methodology encompasses the definition of the base SPM and the selection of the relevant experimental data to be fit the parameter identification scenarios. Second, the boundaries of these scenarios should be established to determine the optimal configuration of the adaptative blocks that better reflect the electrochemical P2D domain.

A. SPM and Experimental Degradation Data

SPM linearises independently each electrode as a single particle [7]. By using Fick's 2nd law equation for spherical diffusivity (1), SPM captures solid particle lithium-ion concentrations $\boldsymbol{C}$ in $\boldsymbol{mol/m^3}$, according to the input flux $\boldsymbol{J}$ at particle boundary, representative radius $\boldsymbol{R}$ and $\boldsymbol{D}$ diffusivity of each positive and negative electrodes [7].

$$\frac{\partial C(r,t)}{\partial t} = \frac{D}{r^2} \cdot \frac{\partial}{\partial r} \cdot \left(r^2 \frac{\partial C(r,t)}{\partial r} \right) \tag{1}$$

System boundaries for the particle flux are defined as:

$$\left. \frac{\partial C(r,t)}{\partial t} \right|_{r=R} = J = \frac{I_{app}(t)}{F \cdot a \cdot L \cdot A} \tag{2}$$

$$\left. \frac{\partial C(r,t)}{\partial t} \right|_{0} = 0 \tag{3}$$

Where $\boldsymbol{I_{app}}$ is the applied current to the cell, $\boldsymbol{F}$ the faraday constant, $\boldsymbol{a}$ electrode's specific interfacial area, $\boldsymbol{L}$ the electrode length, and $\boldsymbol{A}$ the cell plate cross-sectional area.

Nevertheless, solving concentrations with partial differential equation (1) in all points of $\boldsymbol{r}$ is unnecessary for BMS applications. The evaluation point for terminal voltage estimation lies in the concentration at the particle surface $\boldsymbol{C_{ss}} = \boldsymbol{C(r,t)|_{r=R}}$. From all the ROM approaches to reduce computational complexity with LaPlace transforms [9], the present article uses a linearisation based on a Padé approximation that represents equation (1) dynamics with a third-order low-pass filter described in equation (4) for each electrode [13].

$$\frac{C_{ss}(s)}{J(s)} = \frac{\frac{3}{R} + \frac{4 \cdot R}{11 \cdot D} s + \frac{R^3}{165 \cdot D^2} s^2}{s \left(1 + \frac{3 \cdot R^2}{55 \cdot D} s + \frac{R^4}{3465 \cdot D^2} s^2 \right)} \tag{4}$$

Then, the results obtained of mass transfer variation in the particle surface can be used to compute each electrode Open Circuit Potential (OCP). Additionally, concentration values are also used in SPM to calculate each Solid Electrolyte Interphase (SEI) charge transfer resistance represented by the overpotential voltage drop $\boldsymbol{\eta_r}$, defined in equation (5) [9].

$$\eta_r = \frac{2RT}{F} \cdot sinh^{-1}\left(\frac{I_{app}(t)}{2 \cdot a \cdot L \cdot i_0}\right) \tag{5}$$

Where $\boldsymbol{R}$ is the universal gas constant, $\boldsymbol{T}$ the ambient temperature, and $\boldsymbol{i_0}$ is electrode total exchange current density represented in equation (6). In which, $\boldsymbol{k_r}$ is the reaction rate constant, $\boldsymbol{C_e^0}$ the constant electrolyte concentration in SPM concept and $\boldsymbol{C_{s,max}}$ the maximum concentration in the electrode.

$$i_0 = k_r \cdot \sqrt{C_e^0 \cdot C_{ss}(t)(C_{s,max} - C_{ss}(t))} \tag{6}$$

The difference between positive and negative electrode OCP and $\boldsymbol{\eta_r}$ provides the terminal voltage, simulated by SPM.

$$V_t = OCP^+(t) - OCP^-(t) + \eta_r^+ - \eta_r^- \tag{7}$$

The ROM SPM concept represented in this section serves as a foundation for incorporating diverse adaptive filter-based approaches into BMS. However, another key aspect for this purpose is the initial electrochemical parameterisation associated [7].

Chen et al. [15] experimental electrochemical characterisation of LGM50-T is one of the most used in P2D research. The present study uses the parameters in (Table I), equation (8) and equation (9) that relates OCPs depending on the stoichiometric values considering $\boldsymbol{y = C_{ss}^+/C_{s,max}^+}$ for the positive electrode and $\boldsymbol{x = C_{ss}^-/C_{s,max}^-}$ for the negative as SPM initial inputs.

Table I. - Chen et al. [15] reference parameter set.

Parameter	Units	$^+$Electrode	$^-$Electrode
$\boldsymbol{R}$	µm	5.22	5.86
$\boldsymbol{D}$	$\boldsymbol{m^2 \cdot s^{-1}}$	$4 \cdot \boldsymbol{10^{-15}}$	$3.3 \cdot \boldsymbol{10^{-14}}$
$\boldsymbol{L}$	µm	75.6	85.2
$\boldsymbol{a}$	$\boldsymbol{m^{-1}}$	$3.81 \cdot \boldsymbol{10^5}$	$3.84 \cdot \boldsymbol{10^5}$
$\boldsymbol{A}$	$\boldsymbol{m^2}$	0.1027	0.1027
$\boldsymbol{C_{s,max}}$	$\boldsymbol{mol \cdot m^{-3}}$	63104	33133
$\boldsymbol{C_e^0}$	$\boldsymbol{mol \cdot m^{-3}}$	1000	1000
$\boldsymbol{k_r}$	$(\boldsymbol{A \cdot m^3 \cdot m^{-2} \cdot mol^{-1}})^{\boldsymbol{1.5}}$	$3.42 \cdot \boldsymbol{10^{-6}}$	$6.48 \cdot \boldsymbol{10^{-7}}$

$$\begin{aligned} OCP^+ = &-0.8090 \cdot y + 4.4875 \\ &-0.0428 \cdot tanh\big(18.5138 \cdot (y - 0.5542)\big) \\ &-17.7326 \cdot tanh\big(15.7890 \cdot (y - 0.3117)\big) \\ &+17.5842 \cdot tanh(15.9308 \cdot (y - 0.3120)) \end{aligned} \tag{8}$$

$$\begin{aligned} OCP^- = 1.9793 &\cdot exp(-39.3631 \cdot x + 0.2482) \\ &-0.0909 \cdot tanh\big(29.853 \cdot (x - 0.1234)\big) \\ &-0.04478 \cdot tanh\big(14.9159 \cdot (x - 0.2769)\big) \\ &-0.0205 \cdot tanh(30.4444 \cdot (x - 0.6103)) \end{aligned} \tag{9}$$

After defining the initial parameterization for the model, it becomes necessary to define the experimental data that the fitting process leverage as a reference for comparison against the model.

The degradation dataset used in this article is extracted from Pozzato et al.'s [16] database. Wherein, a LGM50-T cell undergoes degradation testing through 185 cycles of a UDDS standard profile at 23 ºC [16]. At specific points in the degradation sequence, the cell is submitted to characterization tests. Among these, there are different C/20 discharges, conducted to estimate the robust SoH values according to capacity fade. To avoid the influence of electrolyte dynamics in SPM, these C/20 discharges are the ideal scenario to conduct the SPM parameter identification process [6].

B. Ageing Mechanism Configurations and validation

Similarly, to [12], [13], LS is selected to optimize the residuals from the differences between experimental C/20 discharge voltage values curves and model output modifying SPM's parameters. The parameter identification process implemented in MATLAB [17] iterates running the model and modifying SPM parameters until it finds an acceptable solution that minimises the error. To test a larger set of possibilities the iterative process uses MATLAB's GD method with an interior-point algorithm integrated.

The essence of linking parameter identification processes from adaptive models with the electrochemical P2D ROM domain, hinges on establishing constraints for SPM parameters. These constraints ensure that the iterative fitting outcomes align with physically meaningful values. These boundaries are defined according to the following statements based on LIB degradation effects:

1) *Particle radius.* Both LGM50-T cell Nickel-Manganese-Cobalt (NMC) cathode and Silicon-Graphite (Si-G) anode, are obtained through the implementation of ion beam milling with Scanning Electron Microscopy (SEM) technique from the work of Chen et. al [15]. The boundaries of $\boldsymbol{R}$ in the parameter identification process are defined in Table II according to the original value and the variations expected as degradation progresses. In one hand, it has been observed that Si-G based anodes experience particle radius ($\boldsymbol{R^-}$) length extensions as degradation progresses [14], [18]. On the other hand, during charge-discharge cycles, cathode $\boldsymbol{R^+}$ experiences tensile stresses, leading to particle expansions and contractions [14]. This process contributes to the mechanical degradation of the cathode, causing the loss of electrode active material due to particle cracking and other side effects that decompose the cathode material [14]. The presence of these effects is reflected in battery capacity fading over time.
2) *Solid Diffusivity.* Commonly $\boldsymbol{D}$ varies depending on the electrode stochiometry and degradation stage [15]. In the process of degradation, the growth of the SEI layer, lithium plating, particle cracking and other side reactions intuitively leads to a gradual increase in charge-transfer resistance, which in terms of diffusivity is correlated with a reduction of $\boldsymbol{D}$ values for both electrodes [14]. Then, to set the parameter identification iterations maximum and minimum values for $\boldsymbol{D}$ in each electrode are defined according to Chen et. al [15] measured limits. Lower boundaries are selected with the objective to extend parameter identification degree of freedom.
3) *Initial Concentration* Degradation produces a stoichiometric drift that affects OCP curves (8) and (9). So, SPM initial concentration
   $\boldsymbol{C_{in}}$ at 100% SoC values vary at each electrode [19]. Fig.1. shows graphically these variations [19]. Thus, the assessment in this article also considers $\boldsymbol{C_{in}}$ as an identifiable SPM parameter. The maximum of this values is the original concentration of the model [15]; for the negative electrode the minimum is established according to the resulting SoH measured from the output capacity on each degradation stage to emulate the complementary implementation with external state estimation block [16]. Then, an externally forced boundary varies multiplying the maximum boundary by the current SoH value.
4) *Reaction Rate Constant.* Throughout degradation this parameter presents the same expected behaviour than diffusivity, also due to the same effects [15]. So, $\boldsymbol{k_r}$ maximum boundaries are fixed to the original values and the minimum is set to increase the range of process' degree of freedom.

Table II. – Electrochemical domain physically-correlated limits for the parameter identification process [14].

Parameter	Maximum	Minimum
$\boldsymbol{R^-}$	$6.26\cdot\boldsymbol{10^{-6}}$	$5.83\cdot\boldsymbol{10^{-6}}$
$\boldsymbol{D^-}$	$3.3\cdot\boldsymbol{10^{-14}}$	$1\cdot\boldsymbol{10^{-16}}$
$\boldsymbol{C_{in}^-}$	29866	Ext.*
$\boldsymbol{k_r^-}$	$6.48\cdot\boldsymbol{10^{-7}}$	$5.83\cdot\boldsymbol{10^{-7}}$
$\boldsymbol{R^+}$	$5.36\cdot\boldsymbol{10^{-6}}$	$5.1\cdot\boldsymbol{10^{-6}}$
$\boldsymbol{D^+}$	$4\cdot\boldsymbol{10^{-15}}$	$1\cdot\boldsymbol{10^{-17}}$
$\boldsymbol{C_{in}^+}$	17038	16975
$\boldsymbol{k_r^+}$	$3.42\cdot\boldsymbol{10^{-6}}$	$3.25\cdot\boldsymbol{10^{-6}}$

Note*: Externally forced.

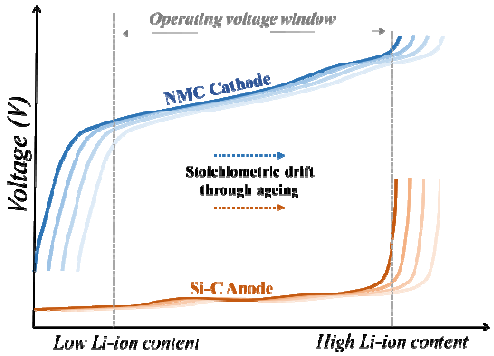

Fig.1. Stoichiometric drift through ageing for LGM50-T cell. Adapted from: [15], [19].

Table III shows the scenarios assessed for each degradation stage that emulate different adaptative block configurations.

Table III. – Emulation scenario configurations

Scenario	R^-	D^-	C_{in}^-	R^+	D^+	C_{in}^+	k_-^+
1	x	x	-	-	-	-	-
2	-	x	x	-	-	-	-
3	-	x	-	-	x	-	-
4	x	x	-	x	x	-	-
5	x	x	x	x	x	x	-
6	x	x	x	x	x	x	x

Scenario 1, emulate the EHM-based adaptative approach implemented by Couto et. al [12] and Goldar et. al [13]; scenario 2, is aimed to highlight the influence of $\boldsymbol{C_{in}}$ as an external fixed variable to roughly emulate a complementary application with a state estimation filtering block; scenario 3, aims to assess the implementation of the positive electrode diffusivity to extend SPM adaptative mechanism capabilities; scenario 4 adds to the previous scenario 3, $\boldsymbol{R^+}$ adjustments to increase the adjustment possibilities within the physical domain; scenario 5 evaluates the consideration of the full SPM parameters and electrodes stoichiometric drift; and scenario 6 adds the assessment of other SPM parameters keys in degradation such as $\boldsymbol{k_r}$.

The following section delves into the results of parameter identification obtained for each scenario across the assessed degradation stages. A study on the performance of the emulated adaptive blocks is conducted to define the optimal configuration. Scenario performance hinges on two crucial factors: accuracy and execution time.

To evaluate accuracy, the Root-Mean-Square-Error (RMSE) is used to compare each parameterized model output with the actual experimental voltage values. Execution time is evaluated by comparing the time needed to fit each scenario to a reduced set of voltage data. The assessment of reduced execution time aligns with real adaptive block implementations practices [9], focusing on the initial 5 seconds of the first degradation stage.

3. Results and Discussion

Fig.2. represents the parameter identification results for SPM base parameters: $\boldsymbol{R}$, $\boldsymbol{D}$ and $\boldsymbol{C_{in}}$.

First, Fig.2. (a) illustrate specific combinations of constrained physical parameters (scenarios 1, 3, and 4) can track diffusivity decay during the identification process. This trend is correlated with physics and holds the potential to be related to SoH fade. Scenarios 2, 5 and 6 reflect that the addition of externally forced variables destabilises diffusivity adjustments complicating the alignment with physically meaningful results.

Fig.2. (b) shows the most significative behaviour followed by the parameter identification algorithm. In scenario 1 base case, the process tries to increase SPM negative particle depletion time, by reducing $\boldsymbol{D^-}$ and $\boldsymbol{R^-}$ in equation (4). These parameter modifications imply that the lower stoichiometric $\boldsymbol{y}$-axis value is reached faster, shifting the cell's terminal voltage cut-off values with equation (9). Then, according to the results, the identification process progressively reduces $\boldsymbol{D^-}$, while keeping $\boldsymbol{R^-}$ nearly constant at its lower boundary. This is because, an increase in $\boldsymbol{R^-}$ affect directly to $\boldsymbol{D^-}$ adjustment trajectory.

Adding more variables to track in the rest of the scenarios make that $\boldsymbol{R^-}$ increase its length. However, Fig.2. (b) slopes do not follow linear fashions, as physics determine [14], [18]. Scenario 4 is the one that better approximates linear behaviour, but the algorithm always tries to converge $\boldsymbol{R^-}$ adjustment to its lower boundary. Therefore, this situation denotes the need of conducting previous test to characterise how the particle radius of each electrode evolve throughout degradation, to properly set Table II boundaries and guide better the parameter identification process. However, these additional tests may require applying multiple complex techniques at different battery cell stages, such as SEM [15].

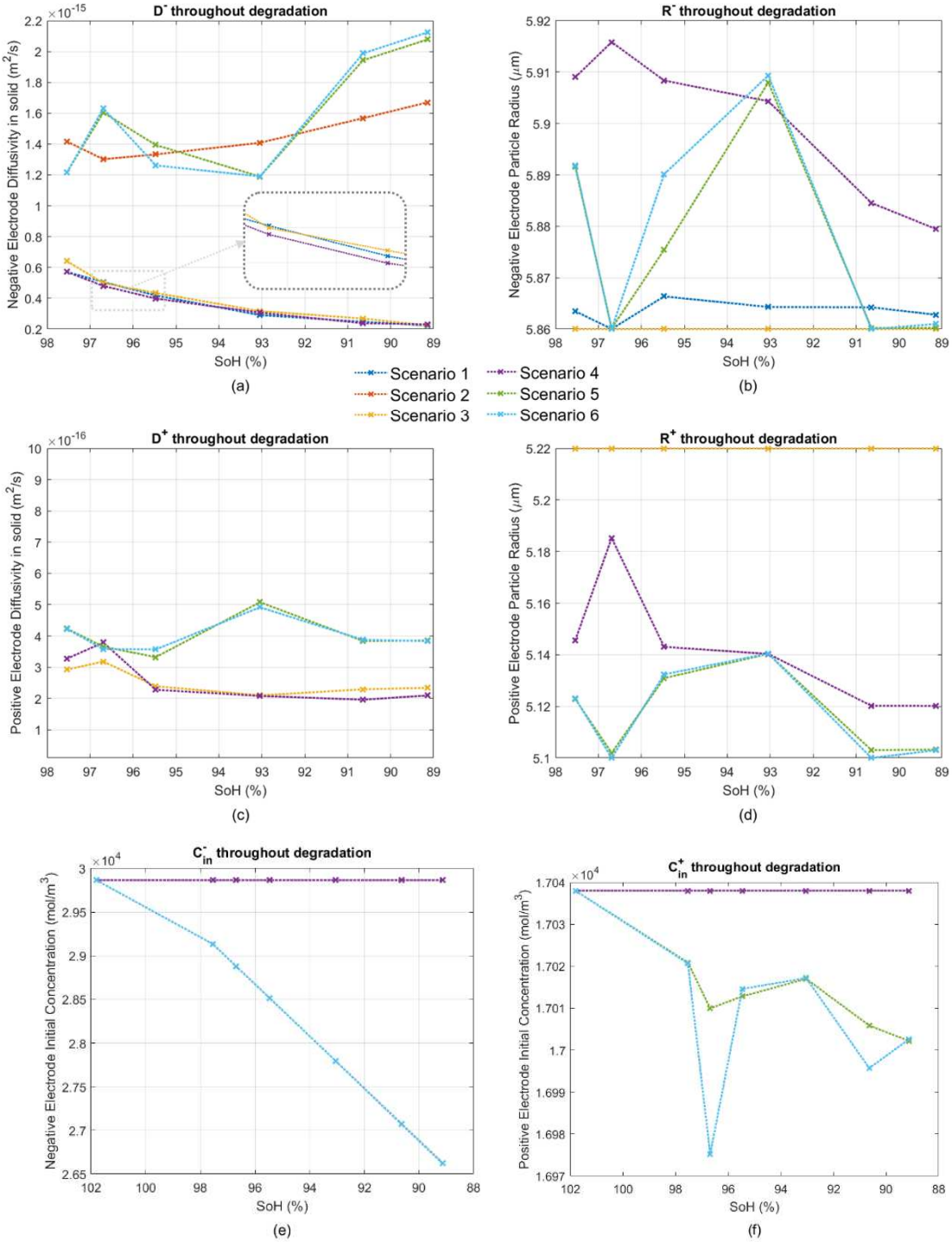

Fig.2. Parameter identification results for the $\boldsymbol{R}$, $\boldsymbol{D}$ and $\boldsymbol{C_{in}}$ configuration of each scenario over degradation stages.

Fig.2. (c) shows how the addition of $\boldsymbol{D^+}$ to the parameter identification process enables a more precise alignment with SoH fading by adjusting equation (8) and (9). Nevertheless, in scenarios 3 and 4 the convergence of $\boldsymbol{D^-}$ and $\boldsymbol{D^+}$ to similar values reflects a more prominent step for $\boldsymbol{D^-}$ adjustments, possibly differing from physics-based expected behaviour, in which the diffusivity decay in both electrodes may follow equivalent trends. However, generally for LIB, the slope of these curves depends always on the electrode material properties. Thus, similarly as in the case of particle radius, diffusivity fade must be experimentally defined according to the degradation stage of each electrode. To do so, charge pulse response tests can be conducted at different SoC, C-rates and temperatures, to further validate the results obtained from identification processes in cell's operative range. However, this deeper analysis also will require the integration of electrolyte dynamics to the SPM model, increasing the number of parameters involved in the identification process [6].

The parameter identification algorithm behaves in Fig.2. (d) as it does in Fig.2. (b), converging to lower boundary setpoint. In this case $\boldsymbol{R^+}$ extended lower boundary in scenarios 4, 5 and 6 enable that $\boldsymbol{R^-}$ growth, approaching physical expectations.

However, an experimental characterisation of $\boldsymbol{R^+}$ throughout degradation is also needed to further align the model with physics.

Fig.2. (e) show how the implementation of $\boldsymbol{C_{in}^-}$ in the identification process, as an external variable, improves RMSE and lowers the weight of SPM parameters in the adaptative process. In scenario 2, 5 and 6, $\boldsymbol{C_{in}^-}$ match exactly SoH fade because in each degradation stage the identification algorithm converges in the lower setpoint for the external variation of $\boldsymbol{C_{in}^-}$ boundary. However, due to this situation, results reflect how the addition of external variables, which are not linearly correlated with SPM equations, destabilise parameter adjustments.

Fig.2. (f) illustrate how the addition of more SPM parameters to adaptative mechanisms overcomplicate the obtention of results aligned with physics, even if the new parameters approximate the expected behaviour as Fig.3. reflects. Besides, as Table IV presents scenario 6 do not provide RMSE improvements in comparison to scenario 5.

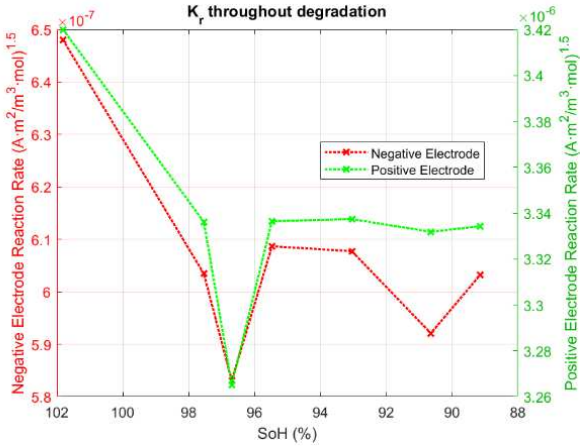

Fig.3. Scenario 6 results for reaction rate constant, adjustments over degradation over degradation stages. Negative electrode $\boldsymbol{k}$ (red left y-axis), Positive electrode $\boldsymbol{k}$ (green right y-axis).

Table IV. – Scenario performance comparison

Scenario:	**1**	**2**	**3**	**4**	**5**	**6**
Mean RMSE	0.06	0.05	0.04	0.04	0.02	0.02
Execution time (s)	10.44	11.25	9.97	14.09	43.80	54.31

Table IV shows how adding parameters to the adaptive mechanism reduces RMSE but increases computational burden. However, simply increasing input parameters does not always improve results physics alignment. Further research is needed to set experimentally parameter boundaries for system validation. Scenarios 2, 5, and 6 remark challenges in combining adaptive mechanisms with state estimation filters. Defining optimal identification algorithm specifications with low computational needs is crucial for compatibility with BMS microcontrollers.

4. Conclusions

The use of diffusivity and particle radius from both electrodes in a parameter identification algorithm, with physically constrained boundaries, has proved its effectiveness tracking diffusivity throughout degradation, in correlation with its expected physical behaviour. Moreover, the improvement regarding base scenario reduces RMSE in 40% without extending algorithm computational demands when only diffusivities are considered as identifiable variables If more physical insight is needed, adding the particle radius to the set of identifiable parameters, then the execution time increases by 30%. These positive results, hold the potential to improve LIB performance and lifespan, enabling more comprehensive model-based SoX indicators within ageing mechanisms, embedded in BMS software.

Acknowledgement

This research was funded by Project PLEC2021-008152, by MCIN/AEI/10.13039/501100011033 and by the European Union "NextGenerationEU"/PRTR", and by the European Union's Horizon 2020 research and innovation programme under grant agreement No 101069765, under the title of IntelLiGent. The authors thank the Catalan Agency AGAUR under their research group support program 2021 SGR 00226. Lluc Canals Casals is a Serra Húnter fellow.

References

[1] M. M. Rana *et al.*, "Applications of energy storage systems in power grids with and without renewable energy integration — A comprehensive review," *J Energy Storage*, vol. 68, p. 107811, Sep. 2023, doi: 10.1016/J.EST.2023.107811.

[2] Y. Yang, E. G. Okonkwo, G. Huang, S. Xu, W. Sun, and Y. He, "On the sustainability of lithium ion battery industry – A review and perspective," *Energy Storage Mater*, vol. 36, pp. 186–212, Apr. 2021, doi: 10.1016/J.ENSM.2020.12.019.

[3] J. P. Rivera-Barrera, N. Muñoz-Galeano, and H. O. Sarmiento-Maldonado, "SoC Estimation for Lithium-ion Batteries: Review and Future Challenges," *Electronics 2017, Vol. 6, Page 102*, vol. 6, no. 4, p. 102, Nov. 2017, doi: 10.3390/ELECTRONICS6040102.

[4] M. F. Ge, Y. Liu, X. Jiang, and J. Liu, "A review on state of health estimations and remaining useful life prognostics of lithium-ion batteries," *Measurement*, vol. 174, p. 109057, Apr. 2021, doi: 10.1016/J.MEASUREMENT.2021.109057.

[5] S. G. Marquis, V. Sulzer, R. Timms, C. P. Please, and S. J. Chapman, "An Asymptotic Derivation of a Single Particle Model with Electrolyte," *J Electrochem Soc*, vol. 166, no. 15, pp. A3693–A3706, Nov. 2019, doi: 10.1149/2.0341915JES/XML.

[6] S. J. Moura, F. B. Argomedo, R. Klein, A. Mirtabatabaei, and M. Krstic, "Battery State Estimation for a Single Particle Model with Electrolyte Dynamics," *IEEE Transactions on Control Systems Technology*, vol. 25, no. 2, pp. 453–468, Mar. 2017, doi: 10.1109/TCST.2016.2571663.

[7] F. Brosa Planella and W. D. Widanage, "A Single Particle model with electrolyte and side reactions for degradation of lithium-ion batteries," *Appl Math Model*, vol. 121, pp. 586–610, Sep. 2023, doi: 10.1016/J.APM.2022.12.009.

[8] K. Liu *et al.*, "Electrochemical modeling and parameterization towards control-oriented management of lithium-ion batteries," *Control Eng Pract*, vol. 124, p. 105176, Jul. 2022.

[9] Y. Li *et al.*, "Model Order Reduction Techniques for Physics-Based Lithium-ion Battery Management: A Survey," 2010, doi: 10.1109/MIE.2021.3100318.

[10] A. Smiley and G. L. Plett, "An adaptive physics-based reduced-order model of an aged lithium-ion cell, selected using an interacting multiple-model Kalman filter," *J Energy Storage*, vol. 19, pp. 120–134, Oct. 2018, doi: 10.1016/J.EST.2018.07.004.

[11] D. C. Vega, S. R. Paz, F. Ornelas-Tellez, and J. J. Rico-Melgoza, "System Parameters' Identification and Optimal Tracking Control for Nonlinear Systems," *IFAC-PapersOnLine*, vol. 51, no. 13, pp. 431–436, Jan. 2018, doi: 10.1016/J.IFACOL.2018.07.324.

[12] L. D. Couto, J. Schorsch, N. Job, A. Léonard, and M. Kinnaert, "State of health estimation for lithium ion batteries based on an equivalent-hydraulic model: An iron phosphate application," *J Energy Storage*, vol. 21, pp. 259–271, Feb. 2019, doi: 10.1016/J.EST.2018.11.001.

[13] A. Goldar, R. Romagnoli, L. D. Couto, A. Romero, M. Kinnaert, and E. Garone, "MPC strategies based on the equivalent hydraulic model for the fast charge of commercial Li-ion batteries," *Comput Chem Eng*, vol. 141, p. 107010, Oct. 2020.

[14] J. S. Edge *et al.*, "Lithium ion battery degradation: what you need to know," *Physical Chemistry Chemical Physics*, vol. 23, no. 14, pp. 8200–8221, Apr. 2021, doi: 10.1039/D1CP00359C.

[15] C.-H. Chen, F. B. Planella, K. O'Regan, D. Gastol, W. D. Widanage, and E. Kendrick, "Development of Experimental Techniques for Parameterization of Multi-scale Lithium-ion Battery Models," *J Electrochem Soc*, vol. 167, no. 8, p. 080534, May 2020, doi: 10.1149/1945-7111/AB9050.

[16] G. Pozzato, A. Allam, and S. Onori, "Lithium-ion battery aging dataset based on electric vehicle real-driving profiles," *Data Brief*, vol. 41, p. 107995, Apr. 2022, doi: 10.1016/J.DIB.2022.107995.

[17] The MathWorks Inc., "MATLAB version: 9.13.0 (R2022b)." The MathWorks Inc., Natick, Massachusetts, United States, 2022. [Online]. Available: https://www.mathworks.com

[18] S. Müller *et al.*, "Quantification and modeling of mechanical degradation in lithium-ion batteries based on nanoscale imaging," *Nature Communications 2018 9:1*, vol. 9, no. 1, pp. 1–8, Jun. 2018.

[19] Y. Merla, B. Wu, V. Yufit, N. P. Brandon, R. F. Martinez-Botas, and G. J. Offer, "Novel application of differential thermal voltammetry as an in-depth state-of-health diagnosis method for lithium-ion batteries," *J Power Sources*, vol. 307, pp. 308–319, Mar. 2016, doi: 10.1016/J.JPOWSOUR.2015.12.122.